SEPTEMBER 2011 VOL 4 NO 9
www.nature.com/naturegeoscience

nature geoscience

EARTH'S HEAT FLUX
Half from radioactive decay

TITAN'S CLOUDS SIMULATED
Precipitation rates high

FIXED-CHANNEL FLOODPLAINS
Bound by early trees

Detached mantle root in the western USA

nature geoscience

LETTERS

PUBLISHED ONLINE: 14 AUGUST 2011 | DOI: 10.1038/NGEO1229

Differential motion between upper crust and lithospheric mantle in the central Basin and Range

Vera Schulte-Pelkum[1]*, Glenn Biasi[2], Anne Sheehan[1] and Craig Jones[1]

Stretching of the continental crust in the Basin and Range, western USA[1], has more than doubled the surface area of the central province[2]. But it is unknown whether stretching affects the entire column of lithosphere down to the convecting mantle, if deep extension occurs offset to the side, or if deeper layers are entirely decoupled from the upper crust[3,4]. The central Basin and Range province is unusual, compared with its northern and southern counterparts: extension began later[1]; volcanism was far less voluminous[5]; and the unique geochemistry of erupted basalts[6–11] suggests a long-preserved mantle source. Here we use seismic data and isostatic calculations to map lithospheric thickness in the central Basin and Range. We identify an isolated root of ancient mantle lithosphere that is ~125 km thick, providing geophysical confirmation of a strong, cold mantle previously inferred from geochemistry[6–8]. We suggest that the root caused the later onset of extension and prevented the eruption of voluminous volcanism at the surface. We infer that the root initially pulled away from the Colorado Plateau along with the crust, but then was left behind intact during extension across Death Valley to the Sierra Nevada. We conclude that the upper crust is now decoupled from and moving relative to the root.

The average surface elevation of the Basin and Range abruptly decreases by 1 km going south across 37° N latitude (Fig. 1a). As crustal thicknesses were not known in detail, estimates of the relative contributions of crust and mantle to surface elevation have been speculative so far[3,12]. We mapped crustal thickness across the area in detail, using EarthScope Transportable Array and Southern Great Basin Digital Seismic Network stations, by locating the crust-mantle boundary (Moho) using P to S converted waves[13] (see Methods and Supplementary Information). If the crust is in isostatic equilibrium, higher surface elevations should be underlain by a deeper Moho; deviations from crustal isostasy may be ascribed to isostatic or dynamic mantle density structure[14].

We find the expected balance of crustal thickness and Moho depth for the high elevations north of 37° N and a shallower Moho south of 36° N, where elevations are low (Fig. 1b), contrary to previous estimates based on sparse Moho depth observations[3,12]. However, the Moho arrivals between 36° and 37° N and between 116° and 118° W are unusually late (Fig. 2b), implying a deep Moho or slow crustal seismic velocities under the low elevations in that area. Neither is reconcilable with crustal isostasy, as slow seismic velocities correspond with decreases in density[15], so a deep Moho or a slow crustal anomaly to explain the increased S-P times would both require much higher elevations across this area than are observed (Fig. 2a, note the 'missing mountains' between stations AMD to BTW; see Methods for calculation). To explore the crustal velocity–density trade-off, we compare the observed crustal density scaled[15] from refraction crustal velocities[3] (Fig. 2c) to the crustal density required to achieve isostatic compensation with no mantle contribution while satisfying the observed Moho delay times, crustal velocity–density relationships[15] and smoothed station elevations (Fig. 2d; see Methods for equations). The lithospheric mantle thickness is fixed to 20 km beneath the Moho everywhere so that no lateral variation of the mantle contribution to surface elevation is allowed, and the lithosphere–asthenosphere density contrast is set to 0.05 g cm^{-3}. The very high average crustal density required in the area of the anomalously late Moho arrivals is roughly opposite to that of the density pattern inferred from crustal refraction (Fig. 2c versus d). Thus, a mantle contribution is required in the area of the Moho root. Observed gravity is consistent with a dense lithospheric mantle root (see Supplementary Information).

We estimate the mantle contribution[16] to surface elevation (Fig. 3a) by subtracting the isostatic contribution of the crust (see Methods), using refraction results to constrain average crustal density and velocities (stars in Fig. 3a) and our complete receiver function results (triangles in Fig. 3a) to constrain Moho depth. We find antibuoyant mantle beneath the Moho root (Fig. 3a), extending from the Nevada Test Site to beneath Death Valley. This anomaly is robust with respect to average crustal densities and velocities, in that we obtain a very similar result when using a constant crustal density and velocities across the study area instead of the refraction data, or when using varying P and S velocities and velocity ratios (see Supplementary Information). We interpret the negatively buoyant mantle anomaly as an at least initially cold and possibly compositionally distinct lithospheric root.

Assuming a lithosphere that is denser than the asthenosphere by 0.05 g cm^{-3} results in a mean lithospheric root thickness of 125 km, compared with a mean of 40 km in the rest of the study area (see Supplementary Fig. S4). To test how realistic the assumption of this fixed density contrast between the lithosphere and asthenosphere is, and to relate density to composition and melting conditions in the mantle, we calculate densities using the pMELTS thermodynamic code[17]. As an endmember model, we first assume a purely thermal density contrast between the lithosphere (conductive geotherm) and asthenosphere (adiabatic geotherm), with no further compositional differences due to depletion of the lithosphere, and use an average asthenospheric dry composition[18]. Resulting mantle density, adiabatic geotherms for two potential temperatures, conductive geotherms for a range of lithospheric thicknesses, and the solidus for this composition are shown in Fig. 3b. We integrate over the density contrast between the adiabat and the conductive geotherm for each lithospheric thickness to calculate the mantle contribution to surface elevation, extrapolating density linearly to pressures and temperatures less than the range for pMELTS shown in Fig. 3b. Figure 3c shows the results of this calculation using the geotherms for the lower mantle potential temperature of 1,300 °C, in comparison to the observed value at each seismic station (values at triangles

[1]Cooperative Institute for Research in Environmental Sciences and Department of Geological Sciences, University of Colorado at Boulder, Boulder, Colorado 80309, USA, [2]Seismological Laboratory, University of Nevada, Reno, Nevada 89557, USA. *e-mail: vera.schulte-pelkum@colorado.edu.

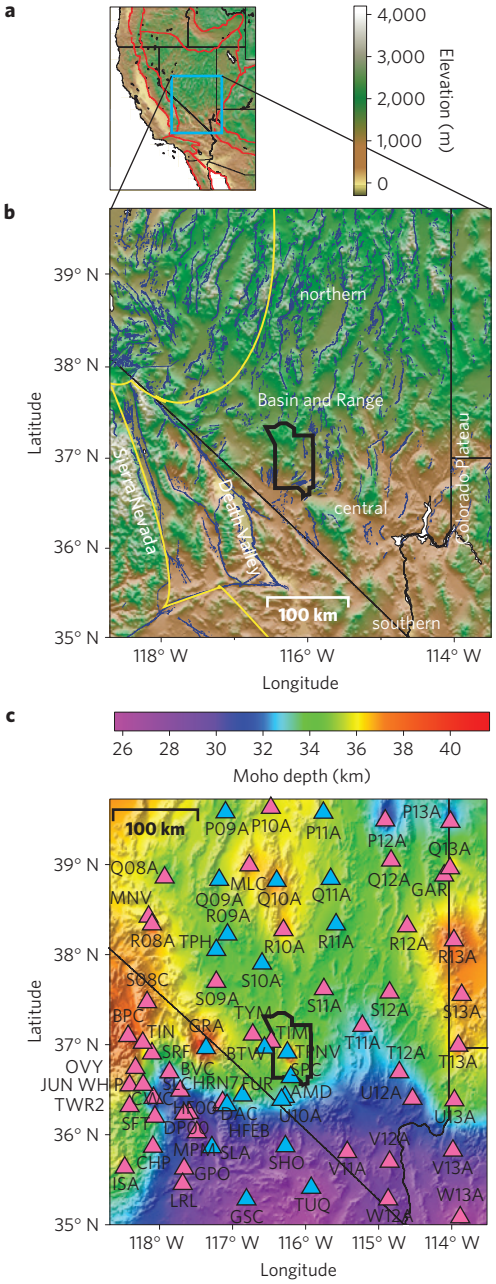

Figure 1 | Location of study area, topography and Moho depths. **a**, Topographic overview map with the study area outlined in blue and tectonic provinces in red. **b**, Topographic map of the study area (note the elevation drop from northern to central Basin and Range). The yellow line is the western edge of the Precambrian craton based on Sr, Nd, and U–Pb isotope studies[28–30]. Faults in blue; Nevada Test Site outlined in black for orientation in subsequent plots. **c**, Moho depth determined from receiver functions (delay times converted to depth using crustal velocities from refraction experiments[3]). Moho is interpolated between values at stations (triangles; stations used in Fig. 2a,b in blue).

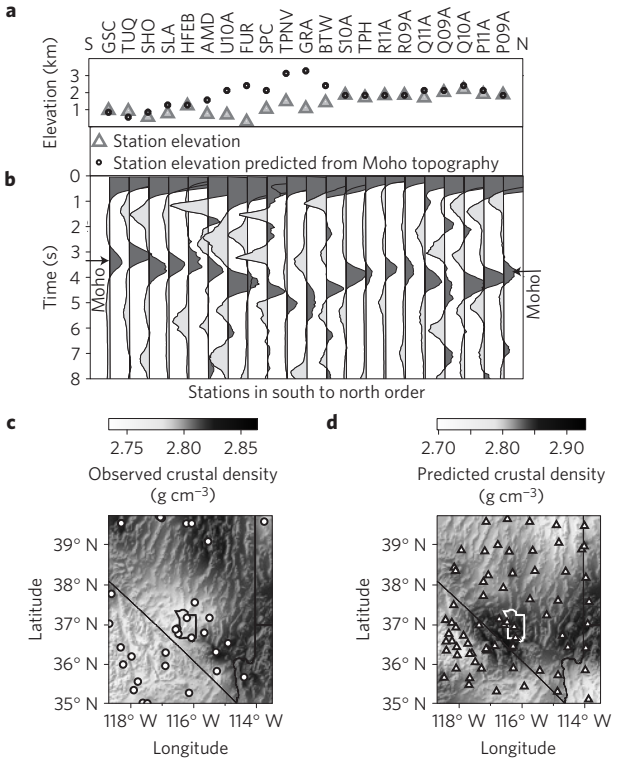

Figure 2 | Lack of isostatic compensation within the crust. **a**, North–south seismic station profile for stations shown in blue in Fig. 1b (selected to cross the anomaly; some noisier stations were omitted) with smoothed (to account for elastic plate thickness[27]) station elevations (grey triangles) and station elevations predicted from Moho topography (black circles, top) assuming isostatic compensation of the crust (see Supplementary Information). **b**, Station average radial receiver functions. **c**, Observed average crustal density scaled from refraction study (circles) P velocities[3]. **d**, Predicted average crustal density from forcing isostatic compensation within the crust while matching Moho delay times at stations (triangles).

in Fig. 3a) projected on a north–south profile. The purely thermal density contrast for this composition would be sufficient to explain surface elevation with a lithospheric root thickness of ~100 km or slightly less (Fig. 3c). However, the lithosphere is probably depleted in major elements relative to the asthenosphere, which reduces its density (for example, by ~0.05 g cm^{-3} for a depleted harzburgite endmember model; see Supplementary Information). The reduction of lithospheric density reduces the amount by which it decreases surface elevation (see Methods, equation (3)), therefore a deeper lithospheric root is needed if it is depleted. Further constraints on the state of the mantle are provided by the observed basaltic magmatism. As there is recent small-volume basaltic magmatism in the area of the root (Fig. 3a,d,e), the geotherm must be in the vicinity of the solidus at some depth. For the asthenospheric composition in Fig. 3b, the geotherm crosses the solidus at 50 km depth. Solidus temperatures increase with major element depletion (see Supplementary Information). Melting in the presence of a much thicker lithosphere requires high asthenospheric temperatures[19] that would put the shallower asthenosphere in the vicinity of the mantle root, well above the solidus (Fig. 3b), resulting in widespread and large-volume volcanism, which is not observed. Hydration or metasomatic enrichment of the lithosphere are mechanisms by which melting can occur at lower temperatures. Direct determination of melting depths and temperatures is difficult, as the erupted basalts are not primary melts (see Supplementary Information). Tomographic images[20,21] show no clear relation to the lithospheric root (see Supplementary Information), which excludes a simple temperature-dependent velocity–density scaling and suggests compositional heterogeneity or the presence of partial melt.

A compositionally distinct lithospheric root is also suggested by the very unusual geochemical signature observed within the area of the antibuoyant mantle[7]. Small-volume basaltic magmatism occurs across most of the study area (Fig. 3a). However, the area of the density anomaly alone yields basalts with very low ε_{Nd} values persisting to present day (Fig. 3d,e). Low ε_{Nd} values in basalts

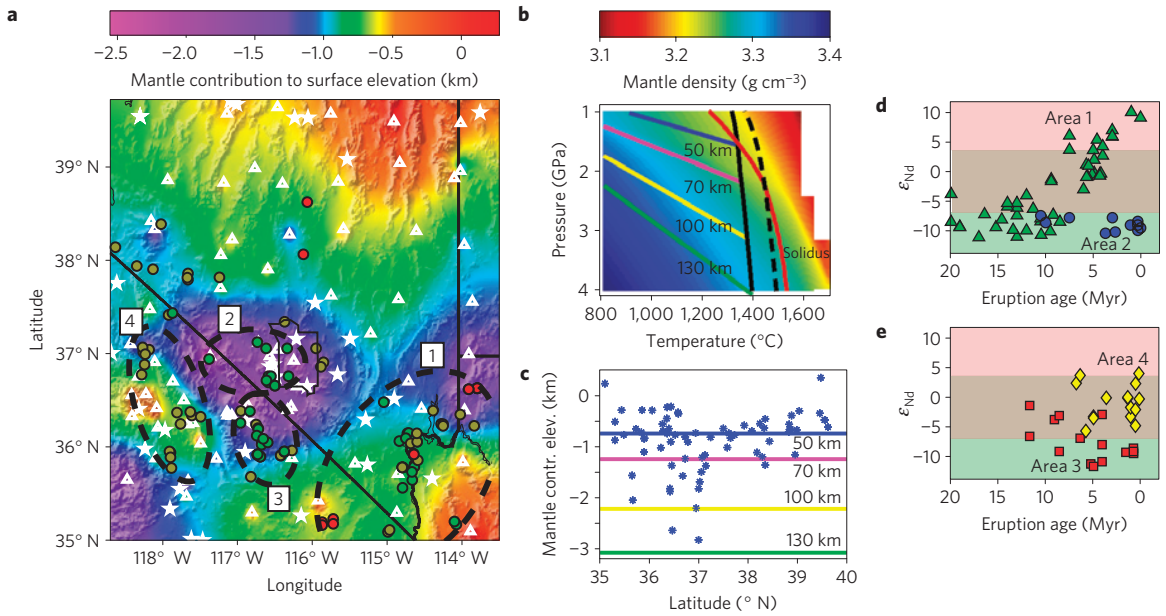

Figure 3 | Mantle buoyancy and basalt geochemistry. a, Map of lithospheric mantle contribution to observed surface elevation. White triangles, station locations; white stars, refraction results. Circles are basalts[6–11] from enriched lithospheric ($\varepsilon_{Nd} < -7$, green), asthenospheric ($\varepsilon_{Nd} > 4$, red), and intermediate (brown) mantle sources. **b**, pMELTS (ref. 17) mantle densities for an average asthenospheric composition[18] and adiabatic (solid black, $T_{pot} = 1{,}300\,^{\circ}C$; dashed, $T_{pot} = 1{,}390\,^{\circ}C$) and conductive geotherms (50–130 km lithospheric thickness); solidus in red. **c**, Predicted (coloured lines) mantle contribution to surface elevation from integration along geotherms ($T_{pot} = 1{,}300\,^{\circ}C$) in **b** compared to observed values (blue stars) at each station shown in **a**, S–N profile. **d**,**e**, Time progression[6] of basalt ε_{Nd} values in areas marked in **a**.

require a long-lived mantle reservoir that has been enriched with trace elements over a long time, whereas basalts derived from convecting asthenosphere have positive ε_{Nd}. Values in basalts of −10 and lower, such as found above the inferred lithospheric root, require that 100% of the Nd in the sample originated in enriched lithospheric mantle[7,8,22]. In the western US, such low values in basalts are only found in the central Basin and Range and otherwise only much further east under Archaean cratons[7]. Within the central Basin and Range, basalts in the Lake Mead extensional area in the east have shifted from similarly low values to asthenospheric values (Area 1, Fig. 3a,d), interpreted as lithospheric removal[6]. Low ε_{Nd} basalts have persisted in the Death Valley extensional area in the west from 12 to 0 Myr ago (Area 2, Fig. 3a,d), with a distribution that matches the geographical extent of the lithospheric root (Fig. 3a). At the southern edge of the lithospheric root, ε_{Nd} values show an unusual decrease with time (Area 3, Fig. 3a,e), implying a shift from a less-enriched lithospheric or mixed lithospheric and asthenospheric source component to an enriched lithospheric mantle source[8]. West of the lithospheric root, ε_{Nd} values show a constant intermediate range (Area 4, Fig. 3a,e).

A pre-extension Precambrian-age lithosphere is likely to be present under the central Basin and Range, based on crustal basement ages (Fig. 1a). The crust (and presumably mantle) north of 37° N and west of 116° W is much younger (Palaeozoic[3]). The Mojave south of 36° N has Precambrian crust, but its lithosphere was modified and eroded during Laramide flat slab subduction, with a northern boundary roughly coinciding with the present day location of the Garlock Fault[23] (Fig. 4). We propose the history illustrated in Fig. 4: (1) An older, thicker, colder lithosphere underlies the central Basin and Range before the beginning of Cenozoic extension. Its presence delays the onset of extension compared to the northern and southern Basin and Range[1], and also prevents the large-volume ignimbrite volcanism prevalent in the northern and southern provinces[5]. (2) When extension initiates in the east, the lithospheric root moves westwards relative to the Colorado Plateau, and the upper crust and mantle beneath the Lake Mead domain

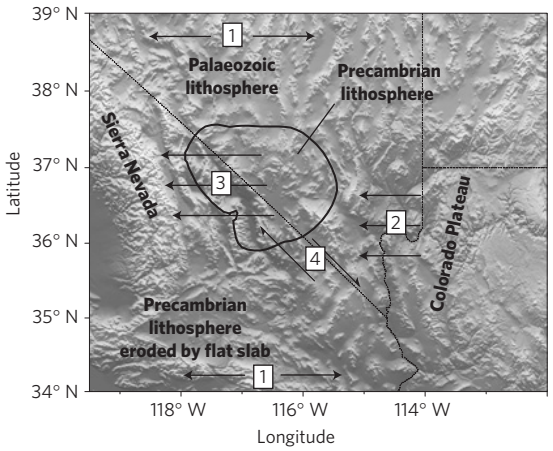

Figure 4 | Tectonic history. Inferred tectonic history sketched on a topographic map (motion arrows not to scale). The black closed shape is the −1 km contour from Fig. 3a (~present day location of lithospheric root). (1) (30–16 Myr; ref. 1) Extension and ignimbrite volcanism in the north and south, hindered by thick Precambrian lithosphere in the central Basin and Range. (2) (16–10 Myr; ref. 1) Breakaway of the root from Colorado Plateau to the west, extension in the Lake Mead domain. (3) (15–0 Myr; ref. 2) Lithospheric root left behind as top-to-west extension in the upper crust jumps to the Death Valley domain. (4) (13–0 Myr; ref. 24) Strike-slip motion carries southern Death Valley upper crust atop Precambrian lithospheric mantle.

undergo concurrent thinning. (3) However, when surface extension then jumps to the western corridor[2], the lithospheric mantle root maintains its position and is left behind while the overlying crust of the Death Valley domain undergoes top-to-the-west extension. (4) Finally, strike-slip motion initiates in the Walker Lane and Eastern California Shear Zone. Along the Stateline fault system east of Death Valley, 30 km of right-lateral offset has been inferred since

13 Myr ago[24]. The distance corresponds to the width of the area that shows decreasing ε_{Nd} values from 12 Myr ago to the present day (Area 3 in Fig. 3a,e). The lithospheric mantle is therefore decoupled from the east–west extension reaching across Death Valley and Panamint and Owens valleys to the Sierra Nevada, as well as from the right-lateral strike-slip motion and north–south shortening in the Walker Lane—Eastern California Shear Zone—Stateline Fault system. Increased lateral warming of the root may result in small-volume basaltic volcanism and gravitational instability[25], similar to the west for the Sierra Nevada, where lithospheric foundering is proposed to have caused uplift of the southern range[26].

Decoupling between the surface and mantle has been proposed for a portion of the northern Basin and Range, ~200 km north of our study area, based on GPS data[4]. Lithospheric thinning under the Lake Mead extensional domain and lateral offset between lithospheric and upper crustal extension in the Death Valley domain were proposed previously based on basalt geochemistry[6]. Two-dimensional lithospheric thickness profiles based on basalt melting depths[6,19] have arrived at lithospheric volumes that require the addition of lithospheric material from outside the central Basin and Range ('distributed shear'[6]), or imply extremely thick pre-extension lithosphere. Our three-dimensional model including decoupling between lithospheric mantle and upper crust and north–south shortening due to strike-slip motion removes some of the lithospheric volume balance problems. Our results present a picture of continental lithospheric deformation that is highly incoherent vertically as well as laterally, where upper crustal deformation can be controlled by pre-existing heterogeneity of strength in the mantle, but can also undergo decoupling from deeper structure, with both processes operating in succession in the same portion of lithosphere.

Methods

Seismic data sets for receiver function analysis were: (1) all broadband data available at the IRIS Data Management Center within the study area, including permanent stations, PASSCAL experiments, and EarthScope Transportable Array stations, from the years 1993–2008; (2) broadband and short-period data from the Southern Great Basin Digital Seismic Network over the years 2000–2007. P arrivals from teleseismic events with a magnitude of $m_b = 5.1$ or greater and within an epicentral range of 28°–99° were selected by a signal-to-noise ratio of the P onset on the vertical component of 3 or above. The time window used in the deconvolution was 20 s before to 30 s after the predicted direct P arrival. We calculated radial and tangential component receiver functions using a time-domain iterative method[13] with a Gaussian filter parameter of three and a minimum variance reduction cutoff of 70%. The results were hand sifted by event and after sorting by azimuth at each station, and we removed radial receiver functions lacking a positive direct P arrival at zero delay and any receiver functions with very large amplitudes or conversions lacking a zero crossing over more than 2.5 s. Results for representative stations are shown in the Supplementary Information. The Moho depths that we obtained by migrating the receiver function Moho delay times with P velocities interpolated between refraction experiment average values[3] and V_p/V_s of 1.73 (Fig. 1c) largely match refraction Moho depths, where those are available (see Supplementary Information).

To predict smoothed station elevations (Fig. 2a) from the Moho delay time observed at the station, we proceeded as follows. If the crust is in isostatic equilibrium, surface topography (T_S) scales to Moho topography (T_M) as $T_S = T_M/C$, where C is the density contrast $\rho_{crust}/(\rho_{mantle} - \rho_{crust})$. A range of crustal densities from 2.73 to 2.8 g cm^{-3} and mantle densities from 3.2 to 3.24 g cm^{-3} only results in variations of a few 100 m in predicted surface elevation, which is much smaller than the discrepancy to actual smoothed surface elevation of >2 km. We choose the most conservative estimate for T_S within the density ranges for mantle and crust. The above isostatic relation only predicts topography, and not absolute elevation. Matching the predicted to the observed elevation for stations with average Moho delay time results in a good fit everywhere except for the anomaly. Choosing different velocities and V_p/V_s ratios for converting Moho delay times to Moho depths has a small effect on the predicted topography, with the anomaly persisting, because changes in velocities and V_p/V_s affect absolute Moho depth to first order but change Moho topography only to second order. The effective elastic thickness of the lithosphere in the Basin and Range is reported as 1.5–15 km (ref. 27), therefore surface elevations should be compensated isostatically when smoothed over a small radius (here, 30 km; using a 50 km radius changes calculated lithospheric thickness insignificantly (<10 km)).

To calculate the crustal and lithospheric mantle contribution to surface topography, we express the smoothed surface elevation ε as the sum of crustal and mantle contributions[3,16], with a constant to bring it into a reference frame at a mid-ocean ridge (2.4 km; ref. 16):

$$\varepsilon = H_{crust} + H_{lithosphere} - H_0 \quad (1)$$

The elevation contribution of each layer is calculated from its thickness L and density ρ:

$$H_{crust} = L_{crust} * (\rho_{asthenosphere} - \rho_{crust})/\rho_{asthenosphere} \quad (2)$$

$$H_{lithosphere} = L_{lithosphere} * (\rho_{asthenosphere} - \rho_{lithosphere})/\rho_{asthenosphere} \quad (3)$$

For Fig. 2d, (lateral crustal variation required to explain the surface elevation with no mantle contribution), we hold lithospheric mantle thickness and density contrast in equation (3) constant. Equation (2) is substituted into equation (1), with the crustal thickness in equation (2) expressed as:

$$L_{crust} = z_{Moho} + \varepsilon \quad (4)$$

$$z_{Moho} = t_{Moho}/(1/v_s - 1/v_p) \quad (5)$$

$$v_p = a + b * \rho_{crust} \quad (6)$$

where z_{Moho} is the Moho depth, t_{Moho} the Moho S-P delay time from receiver functions, v_p the compressional seismic velocity, v_s the shear velocity, and equation (6) a linear velocity–density relationship for crustal materials[15]. We substitute equations (6)–(4) and (2) into equation (1), fix the v_p/v_s ratio to 1.73, and solve the resulting quadratic equation for the average crustal density ρ_{crust} required to satisfy crustal isostasy beneath each seismic station. Parameters for the velocity–density relationship vary with pressure, and therefore with depth, but we found little effect on the result from choosing relations valid for 20 km depth when compared to those for 40 km depth.

To calculate the lithospheric contribution to surface elevation (Fig. 3a), we solve equation (1) for $H_{lithosphere}$. The crustal contribution is calculated using densities scaled from refraction velocities (Fig. 2c). Using a constant average crustal density results in a very similar lithospheric mantle contribution (see Supplementary Information).

Received 2 December 2010; accepted 8 July 2011; published online 14 August 2011

References

1. McQuarrie, N. & Wernicke, B. P. An animated tectonic reconstruction of southwestern North America since 36 Ma. *Geosphere* **1,** 147–172 (2005).
2. Snow, J. & Wernicke, B. Cenozoic tectonism in the Central Basin and Range: Magnitude, rate, and distribution of upper crustal strain. *Am. J. Sci.* **300,** 659–719 (2000).
3. Jones, C. *et al.* Variations across and along a major continental rift—an interdisciplinary study of the Basin and Range province, western USA. *Tectonophysics* **213,** 57–96 (1992).
4. Wernicke, B., Davis, J., Niemi, N., Luffi, P. & Bisnath, S. Active megadetachment beneath the western United States. *J. Geophys. Res.* **113,** B11409 (2008).
5. Eaton, G. The Basin and Range province—origin and tectonic significance. *Annu. Rev. Earth Planet. Sci.* **10,** 409–440 (1982).
6. DePaolo, D. & Daley, E. Neodymium isotopes in basalts of the southwest Basin and Range and lithospheric thinning during continental extension. *Chem. Geol.* **169,** 157–185 (2000).
7. Farmer, G. *et al.* Isotopic evidence on the structure and origin of subcontinental lithospheric mantle in southern Nevada. *J. Geophys. Res.-Solid Earth* **94,** 7885–7898 (1989).
8. Asmerom, Y., Jacobsen, S. & Wernicke, B. Variations in magma source regions during large-scale continental extension, Death Valley region, western United States. *Earth Planet. Sci. Lett.* **125,** 235–254 (1994).
9. Feuerbach, D., Smith, E., Walker, J. & Tangeman, J. The role of the mantle during crustal extension—constraints from geochemistry of volcanic rocks in the Lake Mead area, Nevada and Arizona. *Geol. Soc. Am. Bull.* **105,** 1561–157 (1993).
10. Vaniman, D., Crowe, B. & Gladney, E. Petrology and geochemistry of hawaiite lavas from Crater Flat, Nevada. *Contrib. Mineral. Petrol.* **80,** 341–357 (1982).
11. Rogers, N., Hawkesworth, C. & Ormerod, D. Late Cenozoic basaltic magmatism in the western Great Basin, California and Nevada. *J. Geophys. Res.-Solid Earth* **100,** 10287–10301 (1995).
12. Saltus, R. & Thompson, G. Why is it downhill from Tonopah to Las Vegas? A case for mantle plume support of the high northern Basin and Range. *Tectonics* **14,** 1235–1244 (1995).
13. Ligorria, J. & Ammon, C. Iterative deconvolution and receiver-function estimation. *Bull. Seismol. Soc. Am.* **89,** 1395–1400 (1999).

14. Steinberger, B., Schmeling, H. & Marquart, G. Large-scale lithospheric stress field and topography induced by global mantle circulation. *Earth Planet. Sci. Lett.* **186,** 75–91 (2001).
15. Christensen, N. & Mooney, W. Seismic velocity structure and composition of the continental-crust—a global view. *J. Geophys. Res.-Solid Earth* **100,** 9761–9788 (1995).
16. Lachenbruch, A. & Morgan, P. Continental extension, magmatism and elevation—formal relations and rules of thumb. *Tectonophysics* **174,** 39–62 (1990).
17. Ghiorso, M., Hirschmann, M., Reiners, P. & Kress, V. The pMELTS: A revision of MELTS for improved calculation of phase relations and major element partitioning related to partial melting of the mantle to 3 GPa. *Geochem. Geophys. Geosyst.* **3,** 1030 (2002).
18. Workman, R. & Hart, S. Major and trace element composition of the depleted MORB mantle (DMM). *Earth Planet. Sci. Lett.* **231,** 53–72 (2005).
19. Wang, K., Plank, T., Walker, J. & Smith, E. A mantle melting profile across the Basin and Range, SW USA. *J. Geophys. Res.-Solid Earth* **107,** 2017 (2002).
20. Biasi, G. P. Lithospheric evolution of the Pacific-North American Plate Boundary considered in three dimensions. *Tectonophysics* **464,** 43–59 (2009).
21. Schmandt, B. & Humphreys, E. Seismic heterogeneity and small-scale convection in the southern California upper mantle. *Geochem. Geophys. Geosyst.* **11,** Q05004 (2010).
22. Yogodzinski, G., Naumann, T., Smith, E., Bradshaw, T. & Walker, J. Evolution of a mafic volcanic field in the central Great Basin, south central Nevada. *J. Geophys. Res.-Solid Earth* **101,** 17425–17445 (1996).
23. Luffi, P., Saleeby, J. B., Lee, C-T. A. & Ducea, M. N. Lithospheric mantle duplex beneath the central Mojave Desert revealed by xenoliths from Dish Hill, California. *J. Geophys. Res.-Solid Earth* **114,** B03202 (2009).
24. Guest, B., Niemi, N. & Wernicke, B. Stateline fault system: A new component of the Miocene-Quaternary Eastern California shear zone. *Geol. Soc. Am. Bull.* **119,** 1337–1346 (2007).
25. Elkins-Tanton, L. T. Continental magmatism, volatile recycling, and a heterogeneous mantle caused by lithospheric gravitational instabilities. *J. Geophys. Res.-Solid Earth* **112,** B03405 (2007).
26. Zandt, G. *et al*. Active foundering of a continental arc root beneath the southern Sierra Nevada in California. *Nature* **431,** 41–46 (2004).
27. Lowry, A., Ribe, N. & Smith, R. Dynamic elevation of the Cordillera, western United States. *J. Geophys. Res.-Solid Earth* **105,** 23371–23390 (2000).
28. Kistler, R. & Peterman, Z. Variations in Sr, Rb, K, Na, and initial Sr-87-Sr-86 in mesozoic granitic rocks and intruded wall rocks in Central California. *Geol. Soc. Am. Bull.* **84,** 3489–3511 (1973).
29. Farmer, G. & DePaolo, D. Origin of Mesozoic and Tertiary granite in the western United States and implications for pre-Mesozoic crustal structure: 2. Nd and Sr isotopic studies of unmineralized and Cu-mineralized and Mo-mineralized granite in the Precambrian craton. *J. Geophys. Res.* **89,** 141–160 (1984).
30. Coleman, D., Barth, A. & Wooden, J. Early to Middle Proterozoic construction of the Mojave province, southwestern United States. *Gondwana Res.* **5,** 75–78 (2002).

Acknowledgements

We thank P. Luffi for providing density, entropy, and thermobarometry calculations; B. Schmandt for providing a tomographic model; G. L. Farmer for discussions; B. Wernicke for comments; A. Dean, M. Pettit, J. Ball and C. Vockrodt for assistance with data processing and plots; and the US National Science Foundation for support. A. Dean and M. Pettit were funded in part by the Incorporated Research Institutions for Seismology's summer internship program. Maps were produced with GMT.

Author contributions

A.S. and G.B. initiated the seismic data exchange. G.B. contributed SGBDSN data and tomographic models. A.S. assisted with initial seismic data acquisition and analysis. C.J. pointed out the geographic correspondence between the isostatic results and basalt geochemistry and contributed the compilation of refraction experiment results. V.S-P. performed the seismic and isostatic analysis and wrote the paper. All authors discussed the results and commented on the paper.

Additional information

The authors declare no competing financial interests. Supplementary information accompanies this paper on www.nature.com/naturegeoscience. Reprints and permissions information is available online at http://www.nature.com/reprints. Correspondence and requests for materials should be addressed to V.S-P.

nature geoscience

SUPPLEMENTARY INFORMATION

DOI: 10.1038/NGEO1229

Differential motion between upper crust and lithospheric mantle in the Central Basin and Range

Vera Schulte-Pelkum[1], Glenn Biasi[2], Anne Sheehan[1], Craig Jones[1]

[1] Cooperative Institute for Research in Environmental Sciences and Department of Geological Sciences, University of Colorado at Boulder; [2] Seismological Laboratory, University of Nevada, Reno

Receiver function analysis

Azimuthal variations in the radial receiver functions and significant coherent transverse arrivals were evident at the majority of stations. We picked the Moho conversion time based on the radial receiver function Moho arrival on azimuthal binned and unbinned plots at each station (rather than relying on any information from multiply converted phases[1,2], which may be distorted by non-1-dimensional effects). Fig. S1 shows examples of azimuthal receiver function sections for stations within and outside the anomaly.

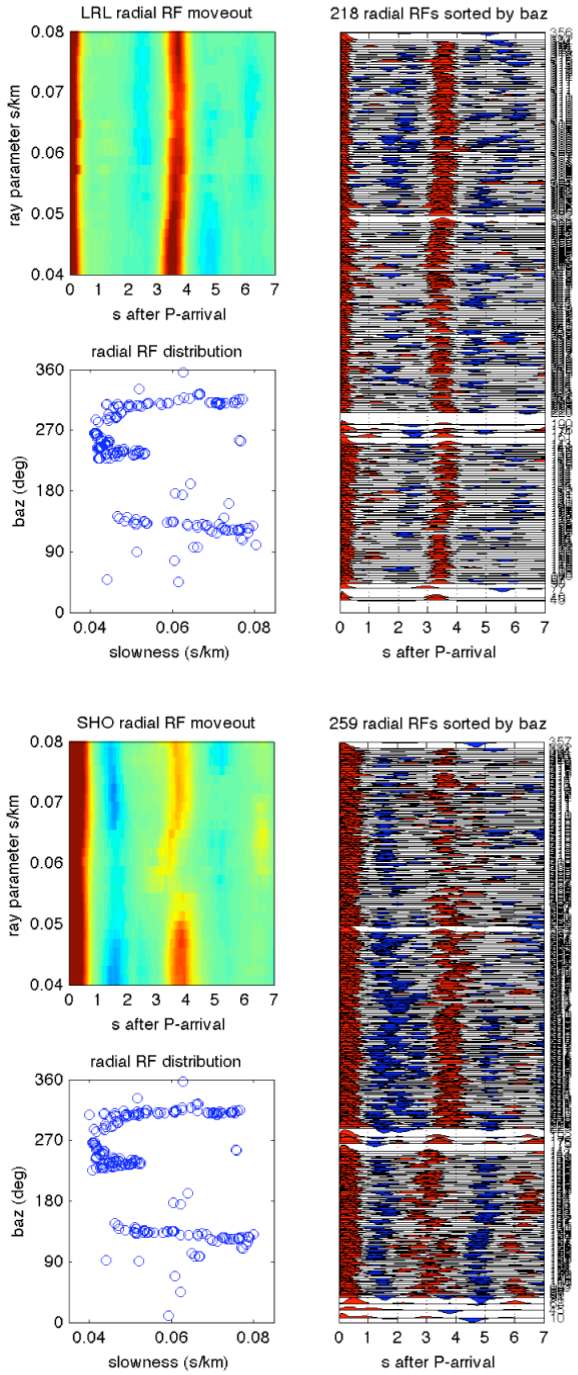

Fig. S1: Moveout plot, source distribution, and radial receiver function section sorted by backazimuth (with elevation and slowness corrections for arrival time and incidence angle correction for amplitude) for two example broadband stations in the south of the study area.

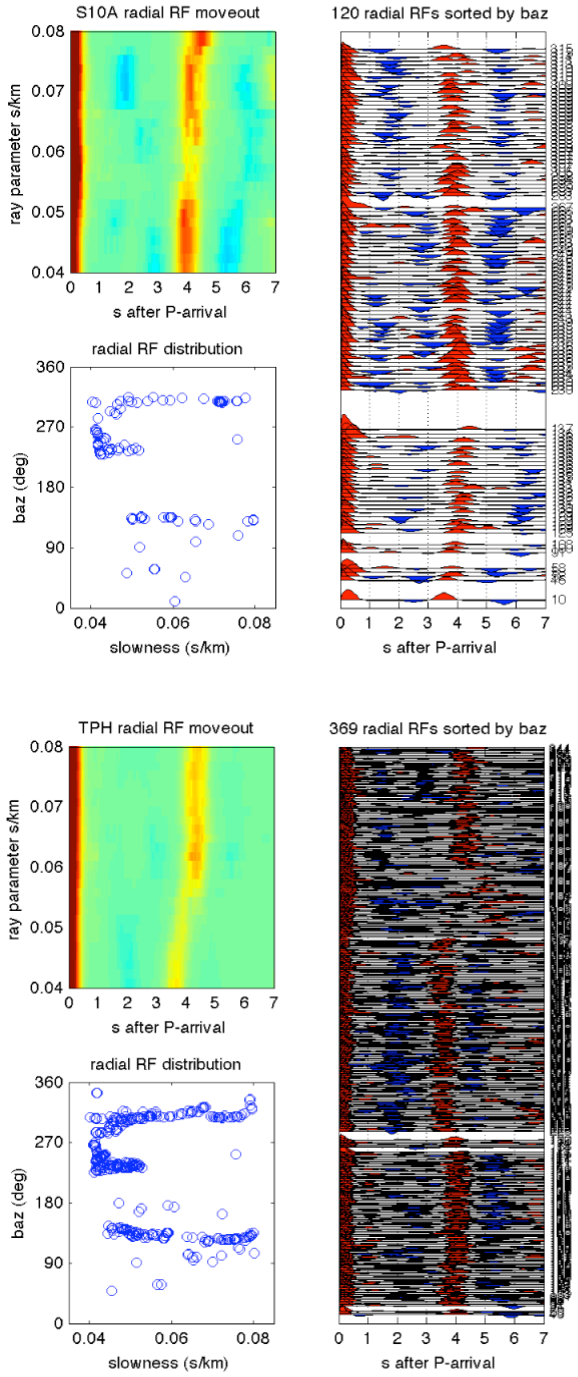

Fig. S1(continued): Two example broadband stations north of the anomaly.

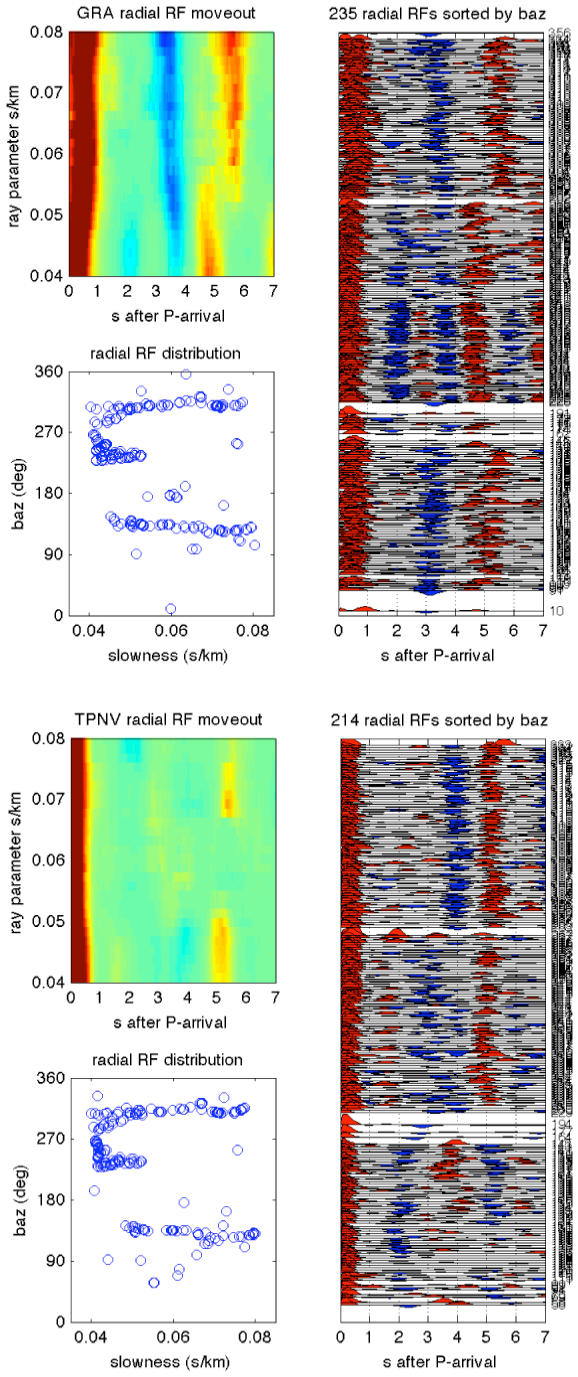

Fig. S1(continued): Broadband stations within the anomaly.

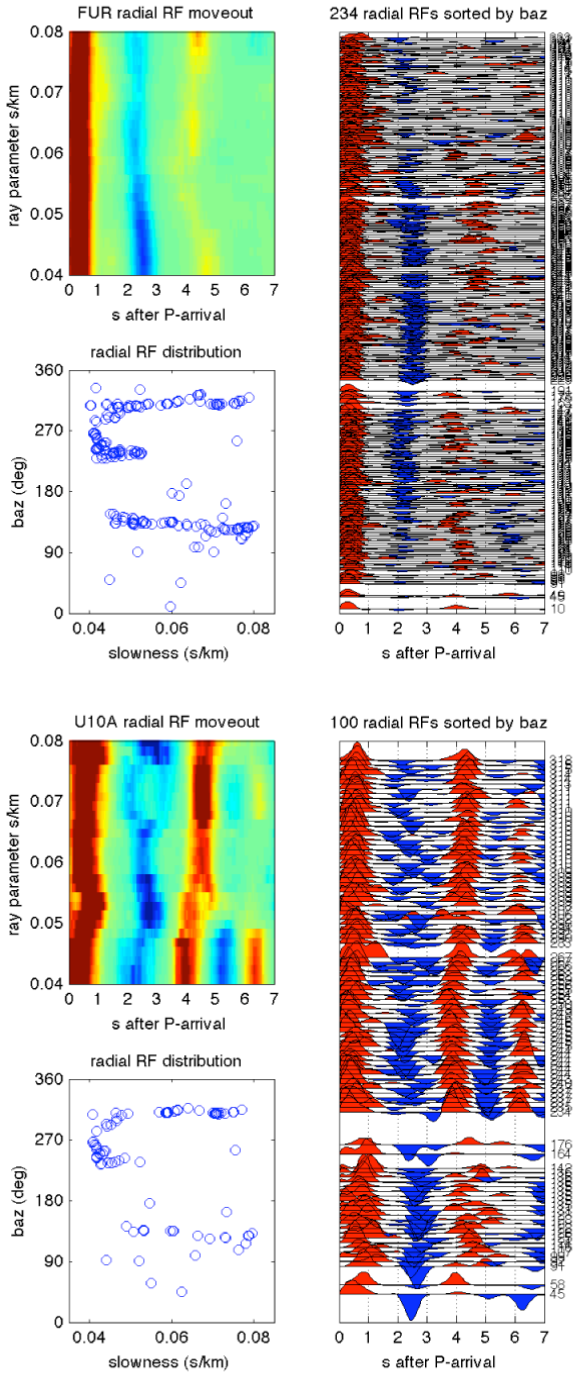

Fig. S1(continued): Broadband stations within the anomaly.

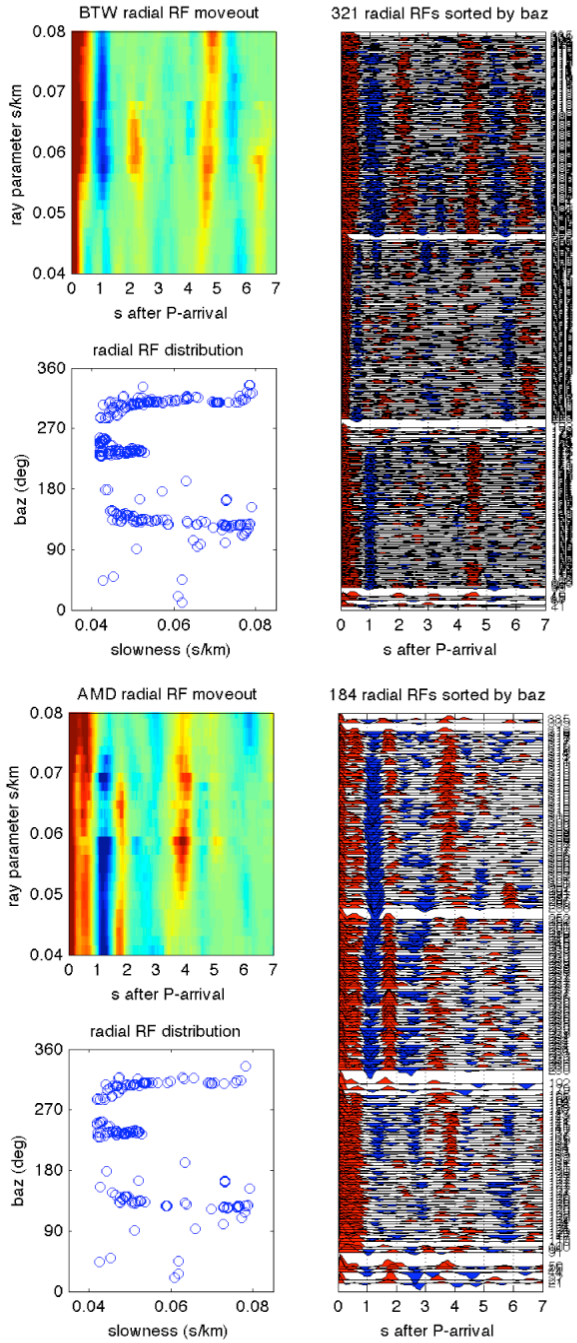

Fig. S1(continued): Short-period stations within the anomaly.

Isostatic elevation calculation

Fig. S2 shows Moho depths from refraction experiments and interpolated between profiles. There is good agreement with depths from the receiver function Moho delay times migrated using the interpolated refraction values (Fig. 1c).

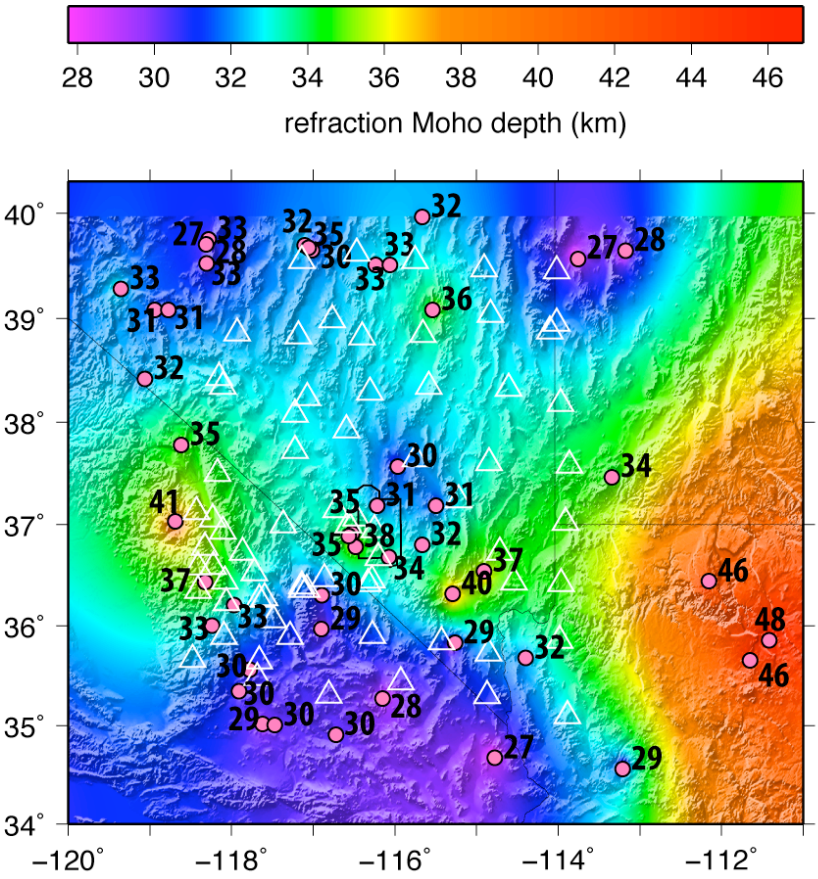

Fig. S2: Moho depths from refraction studies[3]. The average crustal P velocities at these points were interpolated and used to migrate receiver function Moho times at the station locations for this study (white triangles) to obtain the Moho depths shown in Fig. 1c.

Calculation of crustal and mantle contribution to surface elevation

Fig. S3 can be compared to Fig. 3a to illustrate the difference between using a 2-D average crustal density model from refraction profiles and using a constant average crustal density. The difference in the result is small.

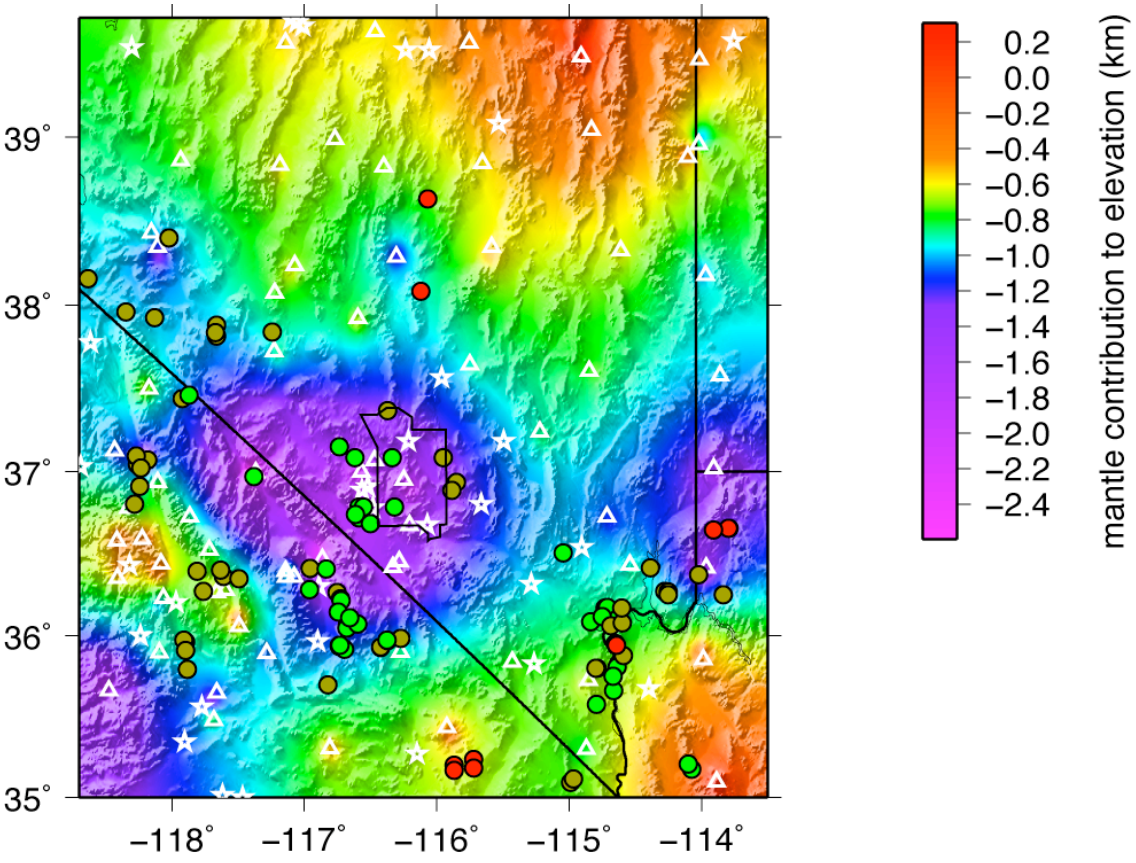

Fig. S3: Lithospheric mantle contribution to surface elevation calculated by assuming constant crustal velocities (Vp = 6.1 km/s, Vp/Vs = 1.73) and density (2.79 g/cm^3) across the study area. Note the similarity to Fig. 3a, where laterally variable crustal parameters were used. Choosing different constant crustal parameters also does not remove the high-density anomaly (Fig. S6, S7).

By assuming density contrasts of the asthenosphere to and lithosphere and correcting fro the crustal contribution, we can solve Eq. 1-3 for the lithospheric mantle thickness (Fig. S5). The calculated lithospheric mantle thickness depends on the assumed density contrasts between crust, lithosphere, and asthenosphere, as well as the assumed average crustal velocity and v_p to v_s ratio used to convert Moho delay times to Moho depth. We use an excess density of 0.05 g/cm^3 for the lithosphere relative to the asthenosphere, which is a standard value (although some estimates range from 0.01 to 0.1 g/cm^3). Crustal velocities increase with density[4], and we calculated the thickness of the anomalous lithosphere using a range of values. The results are shown in Fig. S3. Increasing the average crustal density would reduce the thickness of the lithosphere, so that in principle, the lithosphere anomaly can be minimised in this fashion. However, a higher average crustal density also implies higher seismic velocities, which in turn increases the measured crustal thickness when converting Moho S-P times to Moho depths, which then increases the crustal buoyancy and therefore the thickness of the lithospheric mantle needed to compensate for it. This negative tradeoff makes our result more robust. Fig. 2d shows that to make the anomaly a purely lateral density contrast in the crust, the average crustal density would have to be 2.9 g/cm^3 within the area of the anomaly (with 2.7 g/cm^3 elsewhere), which is an unrealistically high value (in addition, previous refraction profiles have velocities that, when scaled by velocity-density relations[4], show average crustal densities ranging from 2.75 - 2.78 g/cm^3 in this area and no marked contrast to the surroundings). We also performed a similar exercise by varying the v_p to v_s ratio (Fig. S4) and again find that the lithospheric welt is required within a range of acceptable values for the crust.

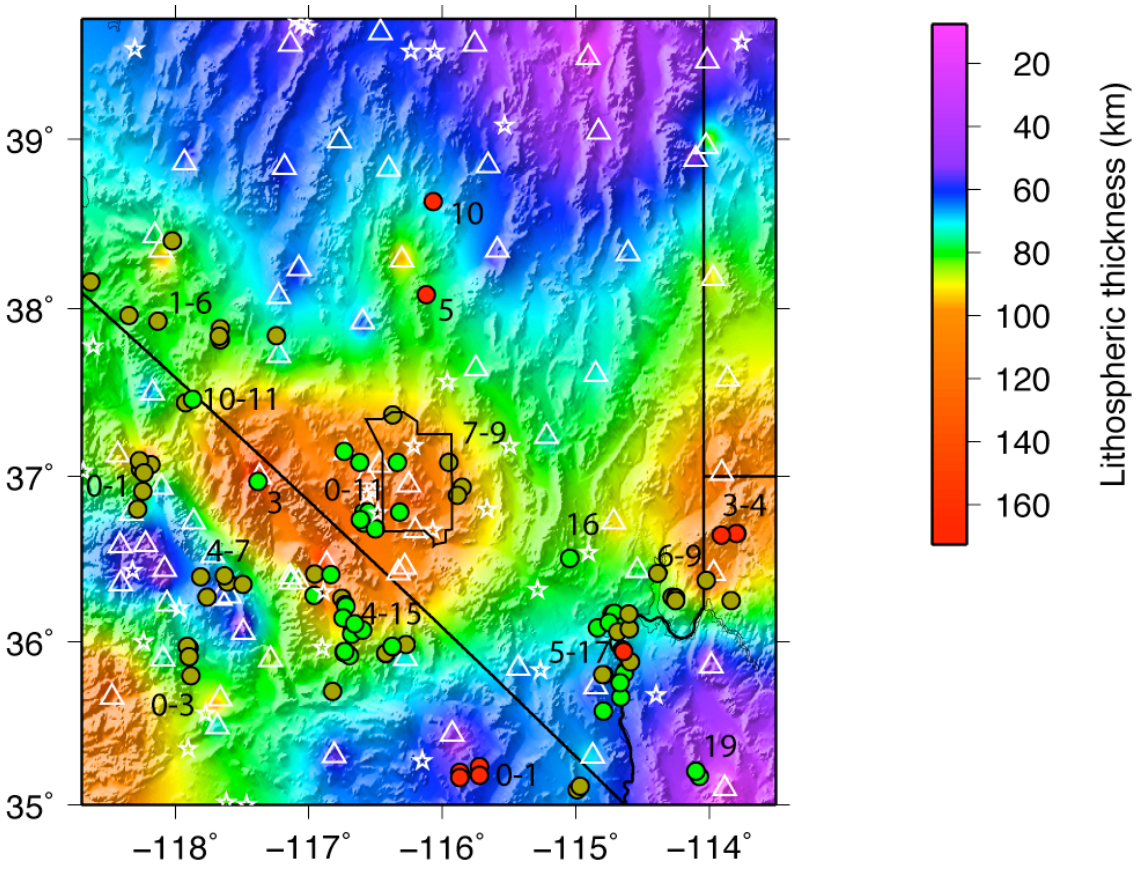

Fig. S4: Lithospheric thickness calculated assuming isostasy and a lithospheric mantle that is denser than the asthenosphere by 0.05 g/cm^3, and using crustal velocities and densities from refraction studies. Symbols as in Fig. 3a, with ages of basalts indicated in addition.

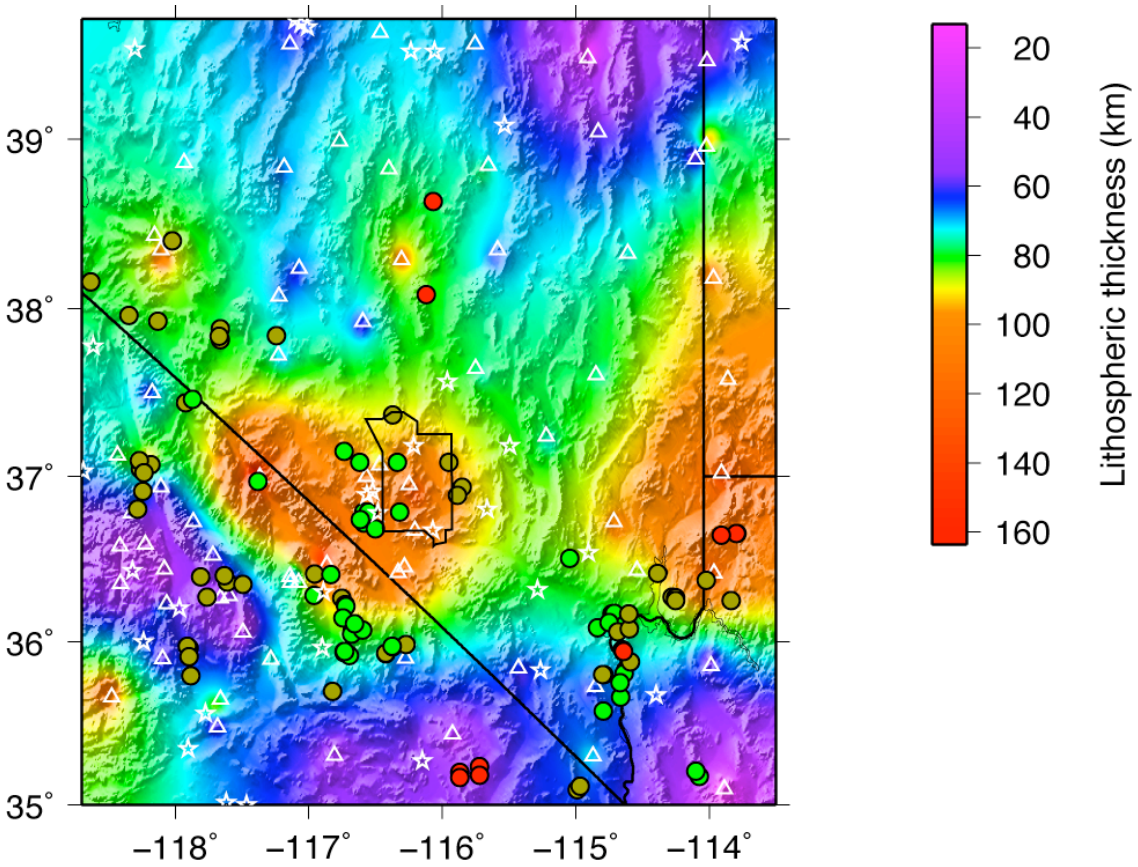

Fig. S5: Lithospheric thickness calculated assuming isostasy and a lithospheric mantle that is denser than the asthenosphere by 0.05 g/cm^3, and using a constant crustal density (2.79 g/cm3) and velocity (6.1 km/s; average of all refraction profiles for both). The central anomaly is very similar to that obtained using the 2-D crustal model (Fig. S4).

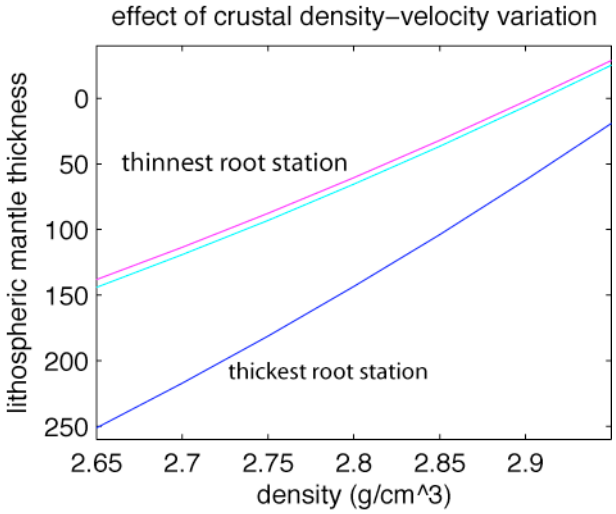

Fig. S6: Effect of crustal density variations on calculated lithospheric thickness. Lateral density variations in the crust (i.e., a denser crust under the anomalous stations) can in principle remove the mantle anomaly. In practice, a denser crust implies faster seismic velocities, which in turn results in a deeper Moho for the same delay time measured with receiver functions, which increases the thickness of crust that has to be compensated, hence requiring a thicker lithosphere. Here, we vary the assumed mean crustal density from 2.65 to 2.95 g/cm^3 (realistic values should fall within 2.75-2.8 g/cm^3) and calculate the lithospheric thickness necessary to put the crust in isostatic equilibrium given the Moho delay time at two stations (maximum and minimum crustal buoyancy within the anomalous region) and using velocity-density relationships[4] for 10 and 40 km depth (which result in nearly indistinguishable lithospheric thicknesses). The lithospheric welt is required within a realistic range of average crustal density.

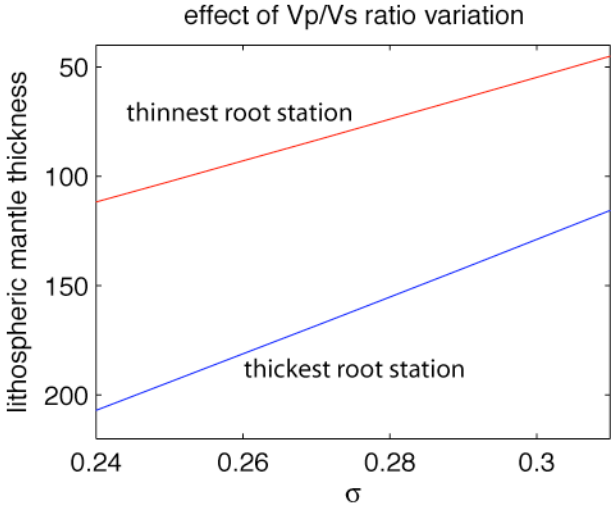

Fig. S7: The same exercise as in Fig. S6 for a range of Poisson's ratios for the crust. Crustal materials should fall within a range of 0.25-0.3.

Petrological calculations of mantle density and solidus

In the following, we integrate density contrast over depth along a variety of geotherms and for some endmember compositions to put constraints on what models can produce the required buoyancy. Fig. 3b shows the case of a purely thermal anomaly. We assume a typical asthenospheric composition ('DMM', slightly depleted mantle[5]) and a potential temperature of 1300^{o}C. Densities, adiabatic geotherms (isoentropes) and solidus are calculated using pMELTS[6]. Depth integration of the density contrast (Fig. 3c) indicates that a minimum lithospheric thickness of over 100 km is needed to explain the observed mantle buoyancy within the density anomaly. The geotherm for such a thick lithosphere is nowhere close to the solidus, so a dry and purely thermal end member model fails to explain the small volume basaltic volcanism.

For a higher potential temperature of 1390^{o}C, the adiabatic geotherm crosses the solidus at 70 km depth. Since there is evidence for much thinner lithosphere in large parts of the Basin and Range, one would expect large volume basaltic volcanism if the potential temperature is indeed this high and if convecting asthenosphere does rise to shallow depths. Since no flood basalts are observed, this is an unlikely end member, as are the much higher potential temperatures proposed elsewhere[7]. Hydration of the mantle brings the solidus to lower temperatures, exacerbating the problem. Thermobarometry based on basalt compositions typically leads to very high melting temperatures and depths in this area, likely reflecting the fact that these are not primary melts (Fig. S8).

Melt depletion of asthenosphere leads to a decrease in density. Fig. S9 shows densities for a depleted end member model, corresponding to highly depleted lithosphere

(harzburgite). The lower densities of a melt-depleted lithosphere would require a much deeper root to fit observed buoyancy. Enrichment of the lithosphere in major and trace elements may explain isotope ratios, volcanism and density contrast best.

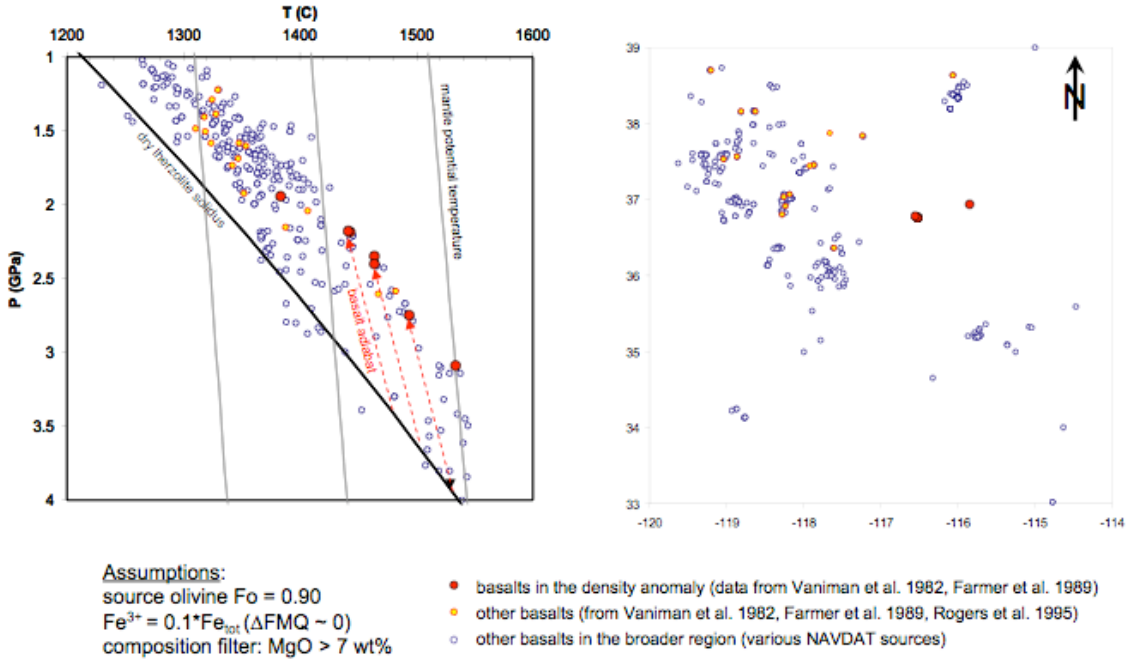

Fig. S8: Estimates for melting temperature and pressure[8]. Figures and calculations provided by Peter Luffi.

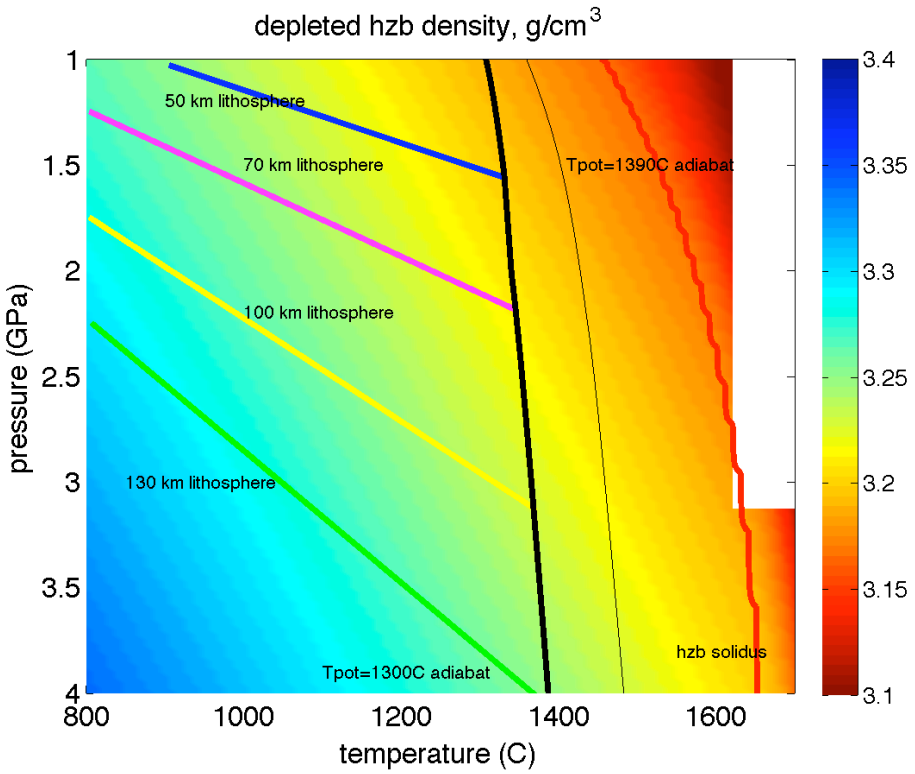

Fig. S9: Same as Fig. S9, but for a depleted harzburgite end member. Melt depletion results in lower densities. pMELTS and isoentrope calculations provided by Peter Luffi.

Tomographic velocity models

Two tomographic studies (teleseismic P) use arrivals from the Southern Great Basin network for sufficient resolution in the area of the density anomaly (the Transportable Array has insufficient station coverage near the Nevada Test Site). Both studies [9,10] image a fast, deep (>170 km) anomaly near the northern part of the Nevada Test Site and suggest that the fast anomaly may be a depleted root remaining after the voluminous Timber Mountain eruptions; however, it could be difficult to create a vertical feature via decompression melting, and maintain its shape over the following 10 Ma. Downwelling lithosphere may be an alternative explanation[10]. Fig. S10 shows velocity perturbation depth slices (top two maps[9], bottom map[10]), overlaid with mantle

buoyant height contours and basalt samples with color coded ε_{Nd} values as in Fig. 3a (station locations are from the buoyancy study and may vary from those used for the tomographic study). Consistent features are a fast anomaly around the northern Test Site and a slow arc to its south and east. The basaltic centers are concentrated on the boundaries between faster and slower seismic velocities, which is possible in association with lateral warming of a lithospheric keel, or with lithospheric downwelling[11].

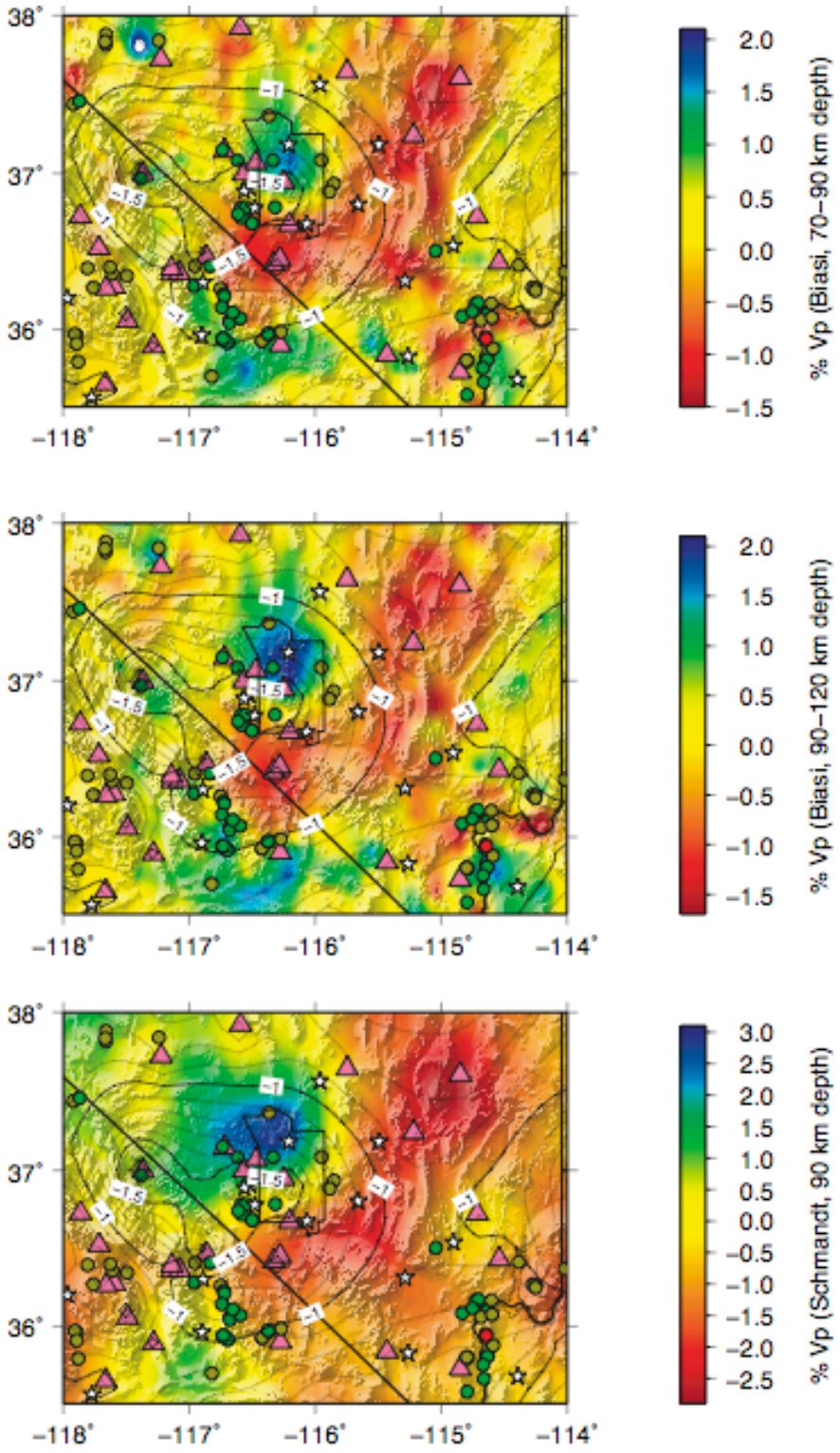

Fig. S10: Teleseismic P velocity tomography results[9,10], overlaid by contours for mantle contribution to elevation as in Fig. 3a. Note the different amplitude scales between the two studies.

Gravity

Free air gravity is dominated by Basin and Range topographic contrasts (Fig. S11) and shows no pronounced low over the density anomaly that may be expected for a dynamic downwelling[12] or an isostatic stable thickened lithosphere; however, this does not rule out either process. The downwarping of the Moho above the mantle density anomaly is expected over a dynamic downwelling[12], but is also consistent with the isostatic case. A dynamic downwelling below a crust of homogeneous viscosity would induce a compressional stress regime in the upper crust and a surface topographic high[12], inconsistent with the observed surface low topography and ongoing East-West extension. The crust throughout the Basin and Range has normal thicknesses despite large extension, in part probably due to lateral transport of lower crustal material[13,14,15], which provides a layer of decoupling between upper crust and the rest of the lithosphere and helps explain the discrepancy between surface and deeper deformation. Zhong[16] (1997) showed that a system with decreased viscosity in the lower crust compared to the upper crust and lithosphere relaxing from a load imposed on the surface or Moho can deviate significantly from the isostatically compensated case. It is therefore unclear whether isostatic compensation should be expected even in the absence of a downwelling (although Zhong's models also favour a crustal keel above a thick lithosphere as we propose here). Unlike the simple 1-dimensional case modelled by Zhong[16] (1997), lateral variations in viscosity and density are also likely in our study area, and their effects on the lithosphere's dynamic response are unknown. The situation in our study area is additionally complicated by ongoing extension and right-lateral strike-slip deformation inducing North-South shortening[17], suggesting that boundary forces may be as important as body forces. Molnar and Houseman[18] (2004) modelled Rayleigh-Taylor instabilities due to convergence and found initial thickening with a

central downwelling, followed by central thinning with paired lithospheric drips at the edges. The lithosphere under the Sierra Nevada just west of our study area is presumed to have foundered recently, causing uplift of the range[19]. Since the downwelling is ~200 km from our observed mantle anomaly and the thinned lithosphere left behind is directly adjacent to it, a consideration of the entire system as a paired downwelling is possible. Bouguer gravity favours a mantle mass excess in the area of the anomaly (Fig. S12, S13), but does not provide a distinction between the isostatic and dynamic cases either. In the absence of independent density and viscosity information, gravity and topography are insufficient for distinguishing between a dynamic and a stable root scenario.

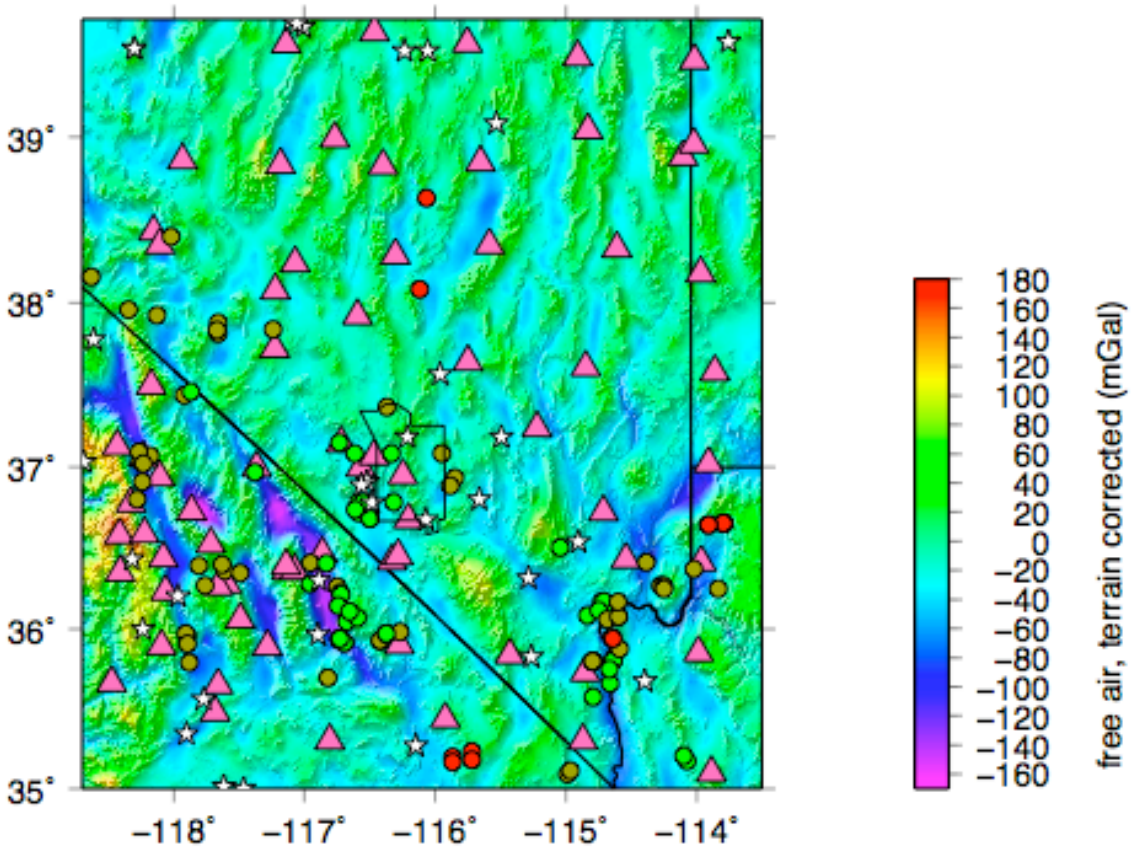

Fig. S11: Terrain corrected free air anomaly. Symbols as in Fig. 3a.

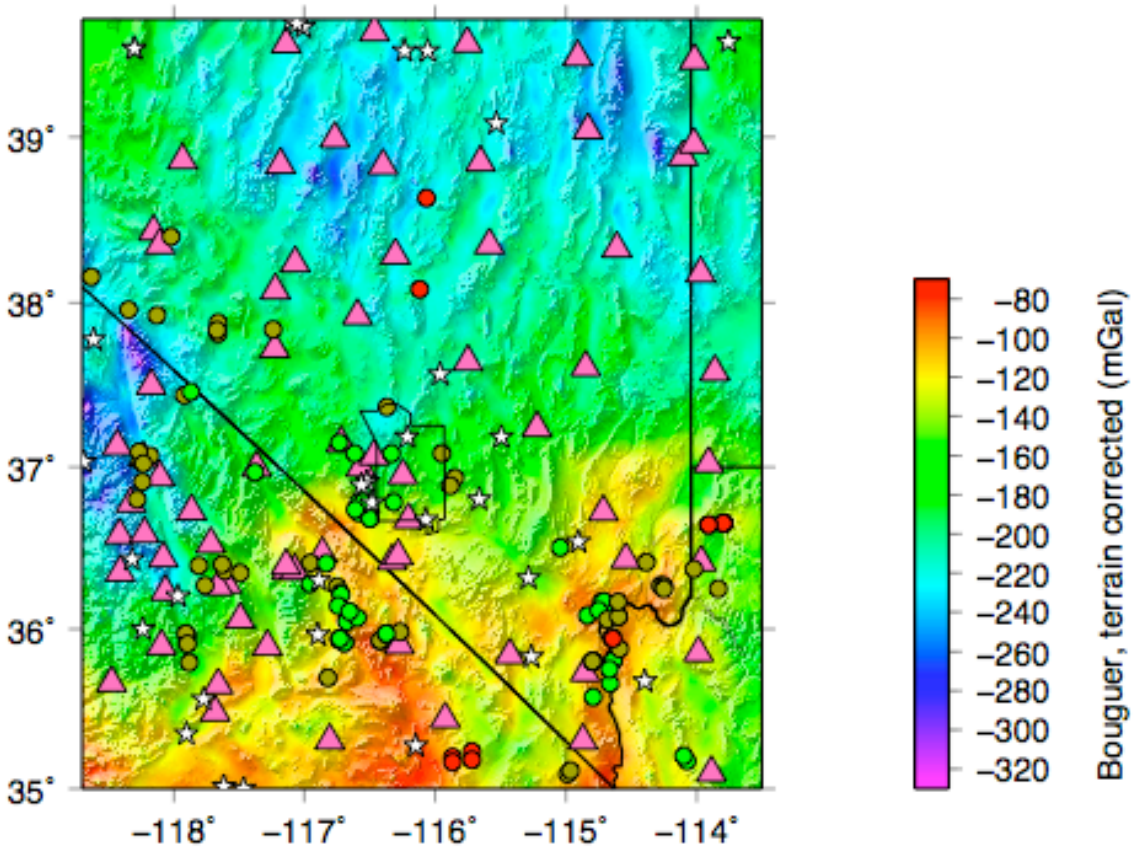

Fig. S12: Terrain corrected Bouguer anomaly. Symbols as in Fig. 3a.

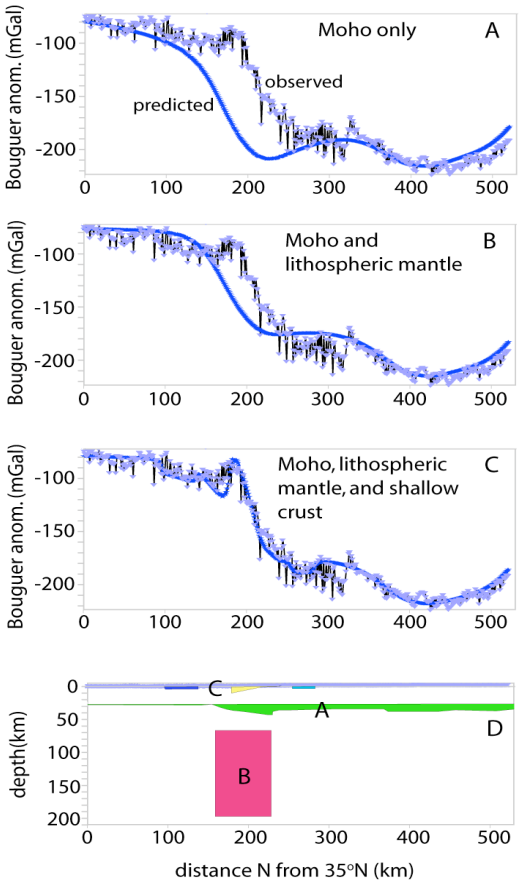

Fig. S13: 2-D gravity modelling and fit to observed Bouguer anomaly (averaged between -116°W and -117°W). (A) predicted (blue) and observed (grey) gravity for observed crustal thickness and elevation alone (green body in (D)). The gradient is reproduced, but at the wrong location. (B) Adding a locally thickened lithosphere removes roughly half of the lateral offset. (C) Adding some known shallow crustal features (Timber Mountain and calderas) allows for a complete fit. The problem is poorly approximated by 2-D geometry and the solution is non-unique, but a structure as derived from isostasy allows fitting the observed gravity. We have been unable to fit the observed gravity without a mantle root underlying the crustal root.

1. Zhu, L. & Kanamori, H. Moho depth variation in southern California from teleseismic receiver functions. *J. Geophys. Res.-Solid Earth* 105, 2969-2980 (2000).

2. Crotwell, H. & Owens, T. Automated receiver function processing. *Seis. Res. Lett.* 76, 702-709 (2005).

3. Jones, C., Wernicke, B., Farmer, G., Walker, J., Coleman, D., McKenna, L., & Perry, F. Variations across and along a major continental rift - an interdisciplinary study of the Basin and Range province, western USA. *Tectonophys.* 213, 57-96 (1992).

4. Christensen, N. & Mooney, W. Seismic velocity structure and composition of the continental-crust - a global view. *J. Geophys. Res.-Solid Earth* 100, 9761-9788 (1995).

5. Workman, R. & Hart, S. Major and trace element composition of the depleted MORB mantle (DMM). *Earth Planet. Sci. Lett.* 231, 53-72 (2005).

6. Ghiorso, M., Hirschmann, M., Reiners, P., & Kress, V. The pMELTS: A revision of MELTS for improved calculation of phase relations and major element partitioning related to partial melting of the mantle to 3 GPa. *G-Cubed* 3, 1030 (2002).

7. Wang, K., Plank, T., Walker, J., & Smith, E. A mantle melting profile across the basin and range, SW USA. *J. Geophys. Res.-Solid Earth* 107, 2017 (2002).

8. Lee, C.-T. A., Luffi, P., Plank, T., Dalton, H., & Leeman, W. P. Constraints on the depths and temperatures of basaltic magma generation on Earth and other terrestrial planets using new thermobarometers for mafic magmas. *Earth Planet. Sci. Lett.* 279, 20-33 (2009).

9. Biasi, G. P. Lithospheric evolution of the Pacific-North American Plate Boundary considered in three dimensions. *Tectonophys.* 464, 43-59 (2009).

10. Schmandt, B. & Humphreys, E. Seismic heterogeneity and small-scale convection in the southern California upper mantle. *G-Cubed* 11, Q05004 (2010).

11. Elkins-Tanton, L. T. Continental magmatism, volatile recycling, and a heterogeneous mantle caused by lithospheric gravitational instabilities. *J. Geophys. Res.-Solid Earth* 112, B03405 (2007).

12. Hoogenboom, T. & Houseman, G. Rayleigh-Taylor instability as a mechanism for corona formation on Venus. *Icarus* 180, 292-307 (2006).

13. Asmerom, Y., Jacobsen, S., & Wernicke, B. {Variations in magma source regions during large-scale continental extension, Death Valley region, western United States}. *Earth Planet. Sci. Lett.* 125, 235-254 (1994).

14. MacCready, T., Snoke, A., Wright, J., & Howard, K. Mid-crustal flow during Tertiary extension in the Ruby Mountains core complex, Nevada?. *Geol. Soc. Am. Bull.* 109, 1576-1594 (1997).

15. Kruse, S., McNutt, M., Phipps-Morgan, J., Royden, L., & Wernicke, B. Lithospheric extension near Lake Mead, Nevada - a model for ductile flow in the lower crust. *J. Geophys. Res.-Solid Earth* 96, 4435-4456 (1991).

16. Zhong, S. Dynamics of crustal compensation and its influences on crustal isostasy. *J. Geophys. Res.-Solid Earth* 102, 15287-15299 (1997).

17. McQuarrie, N. & Wernicke, B. P. An animated tectonic reconstruction of southwestern North America since 36 Ma. *Geosphere* 1, 147-172 (2005).

18. Molnar, P. & Houseman, G. The effects of buoyant crust on the gravitational instability of thickened mantle lithosphere at zones of intracontinental convergence.

Geophys. J. Int. 158, 1134-1150 (2004).

19. Zandt, G., Gilbert, H., Owens, T., Ducea, M., Saleeby, J., & Jones, C. Active foundering of a continental arc root beneath the southern Sierra Nevada in California. *Nature* 431, 41-46 (2004).